Supplementary Material

1 SUPPLEMENTARY TABLES AND FIGURES

1.1 Figures

1.1.1 Example Infrasound Waveforms

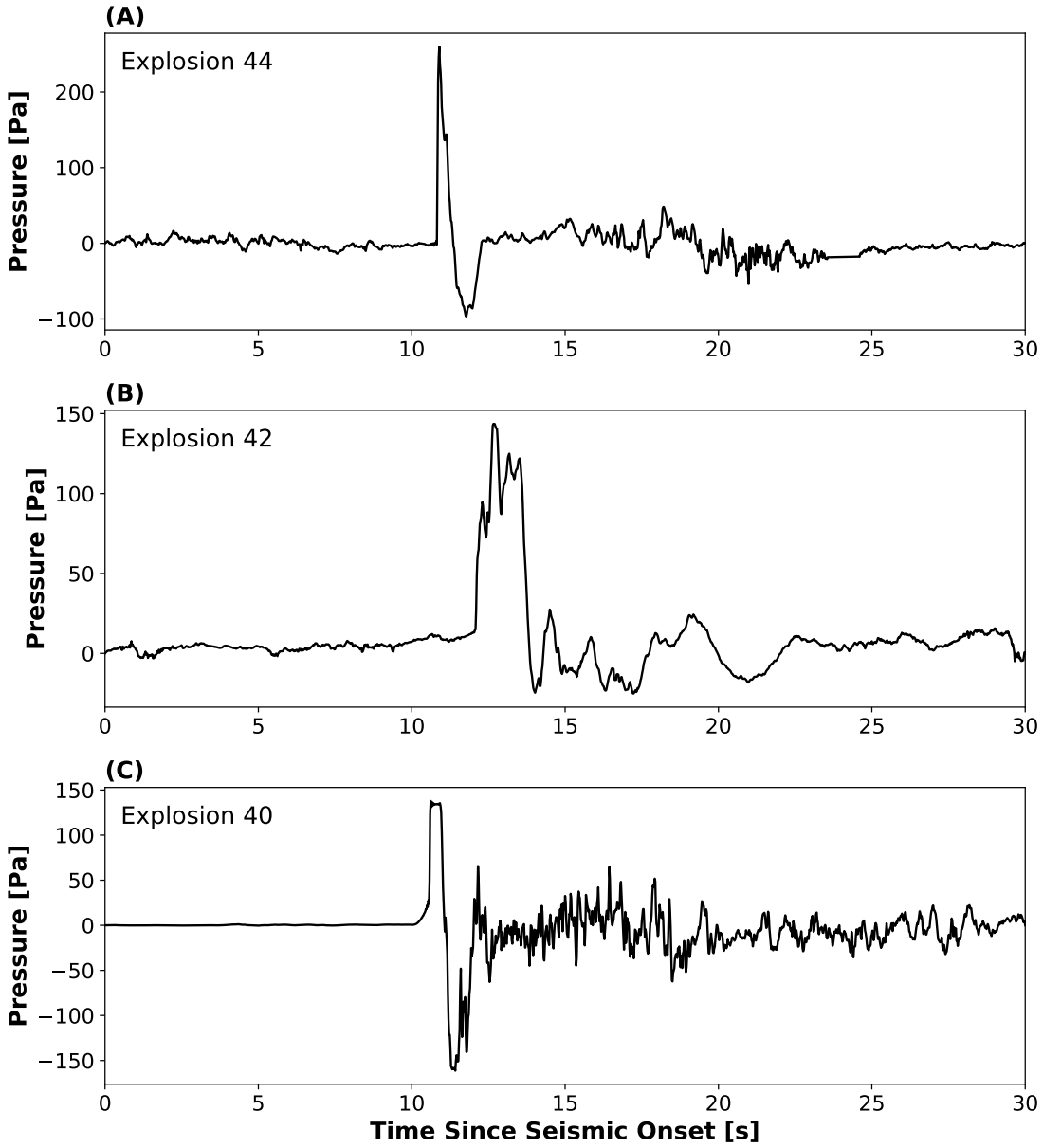

Figure S1. Infrasound waveforms for three explosions discussed in the manuscript to show detail. **(A)** Explosion 44 showing a single main compressional phase. **(B)** Explosion 42 showing multiple compressions in a row. **(C)** Explosion 40 where a preceding low amplitude infrasound phase <0.5 s prior to the main explosion onset is shown.

1.1.2 Arrival Time of Various Seismic Frequency Components

If a bottom-up explosion model is valid at Cleveland, we might expect to see multiple arrivals at the seismometer, the first corresponding to the initiation of the explosion at depth and a second arrival when the dome/plug is exploded at the surface. The frequency content between these arrivals may differ due to the different source processes and be detectable. To examine this possibility the vertical component of CLES seismic data are bandpass filtered in the "low" frequency band (0.25 - 0.5 Hz, which are the lowest frequencies with explosion signals and the frequency band of seismic source inversions by Haney et al. (2019)) and a "high" frequency band (3 - 25 Hz) for example Explosion 45 in Figure S2. The frequency at the onset starts with energy <5 Hz, and gradually increases to < 7 Hz over the course of a few seconds (Fig. S2A). The low and high frequency bands of the seismic explosion signal are shown in the time domain in Figure S2B, where the onset time appears similar, and the ground-coupled airwave is clearly visible as the high frequency arrival after ∼10 seconds.

For most explosions, the low and high frequency energy arrive at or near the same time. The spectrograms show a gradual addition of higher frequency content (Figure S2A), but lack a distinct, quantifiable secondary seismic onset. We find that some explosions, such as Explosion 41, have a measurably different start time for the low frequency seismic energy that precedes the high frequency component, but this is a minority among the explosions in the study. Additionally, there are no examples of the opposite occurring, where the high frequency onset measurably precedes the lower frequency energy. Because of the lack of a clear secondary seismic arrival, we do not include this frequency analysis in our exploration of potential changing explosion source depth.

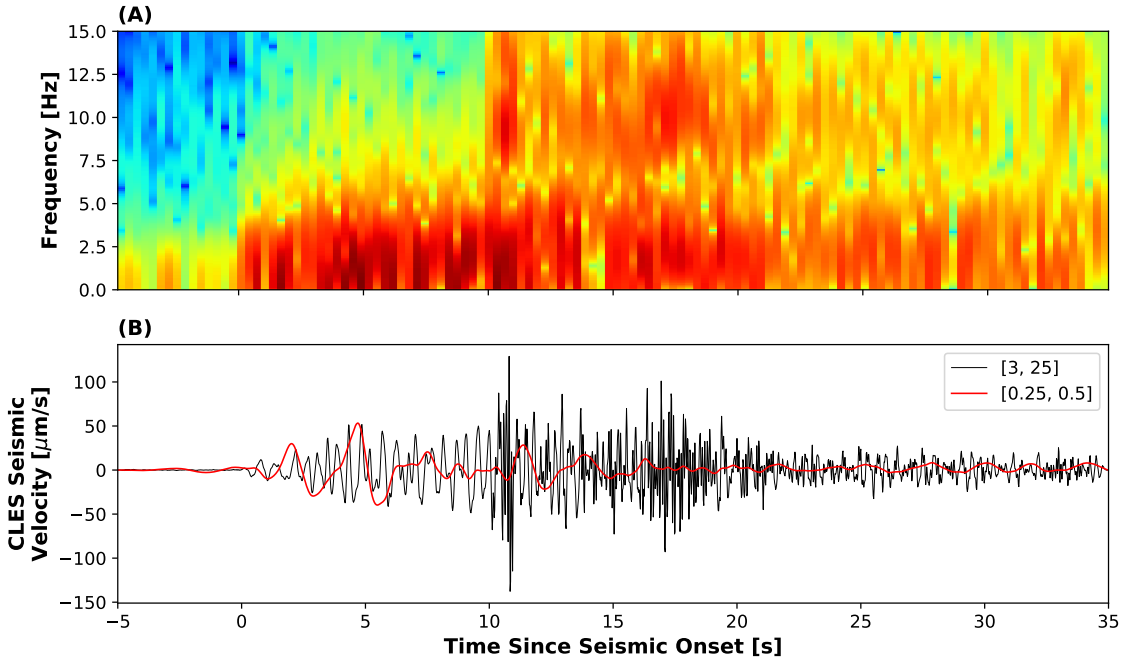

Figure S2. Frequency content breakdown for example Explosion 45. **(A)** Spectrogram of the explosion signal between 0-15 Hz. **(B)** Seismic waveform of the explosion signal in the time domain for multiple frequency bands. The ground-coupled airwave is visible as the high frequency arrival ∼10 seconds after the explosion onset.

1.1.3 CLES/CLCO Seismic Amplitude Ratio

One method we used to investigate the potential changing source depth within the conduit is by taking the ratio of the peak amplitudes of the closer station (CLES) and the surface waves of the distal station (CLCO). This type of analysis draws similarities to the basis of the comparison of body-wave magnitude (M_b) and surface wave magnitude (M_s) for earthquakes (Bath, 1985). Higher values of the ratio may mean relatively more body wave/less Rayleigh wave. If a higher ratio were to correlate with higher positive traveltime residuals, then it may suggest deeper sources that generate less surface wave energy and have longer propagation in the conduit leading to the higher positive values of traveltime residual. Due to the lack of strong correlation and the reliance on a second seismometer, we do not include this analysis in the main paper. We note that this method may be useful for other seismometer configurations at other volcanoes.

We bandpass filter the displacement data between 0.25-0.5 Hz for both stations CLES and CLCO. Then, we find the peak amplitude of the p-wave within a window of 1.5 seconds after the onset on the East component (essentially the first positive bump). Similarly, we find the peak amplitude of the Rayleigh wave in the window of 5 seconds after the surface wave onset on the east component of station CLCO (positive, negative, positive bumps). Then, we divide the peak amplitude value of CLES by the peak amplitude value of CLCO for each explosion. A very weak to no correlation is found between this amplitude ratio and both the seismo-acoustic time lag and the travel time residual (R-squared values of 0.06 and 0.01, respectively, Figure S3a,b). We show the vertical and radial components of CLCO data, highlighting the Rayleigh wave with characteristic 90 degree phase shift, for example Explosion 44 in Figure S3c,d.

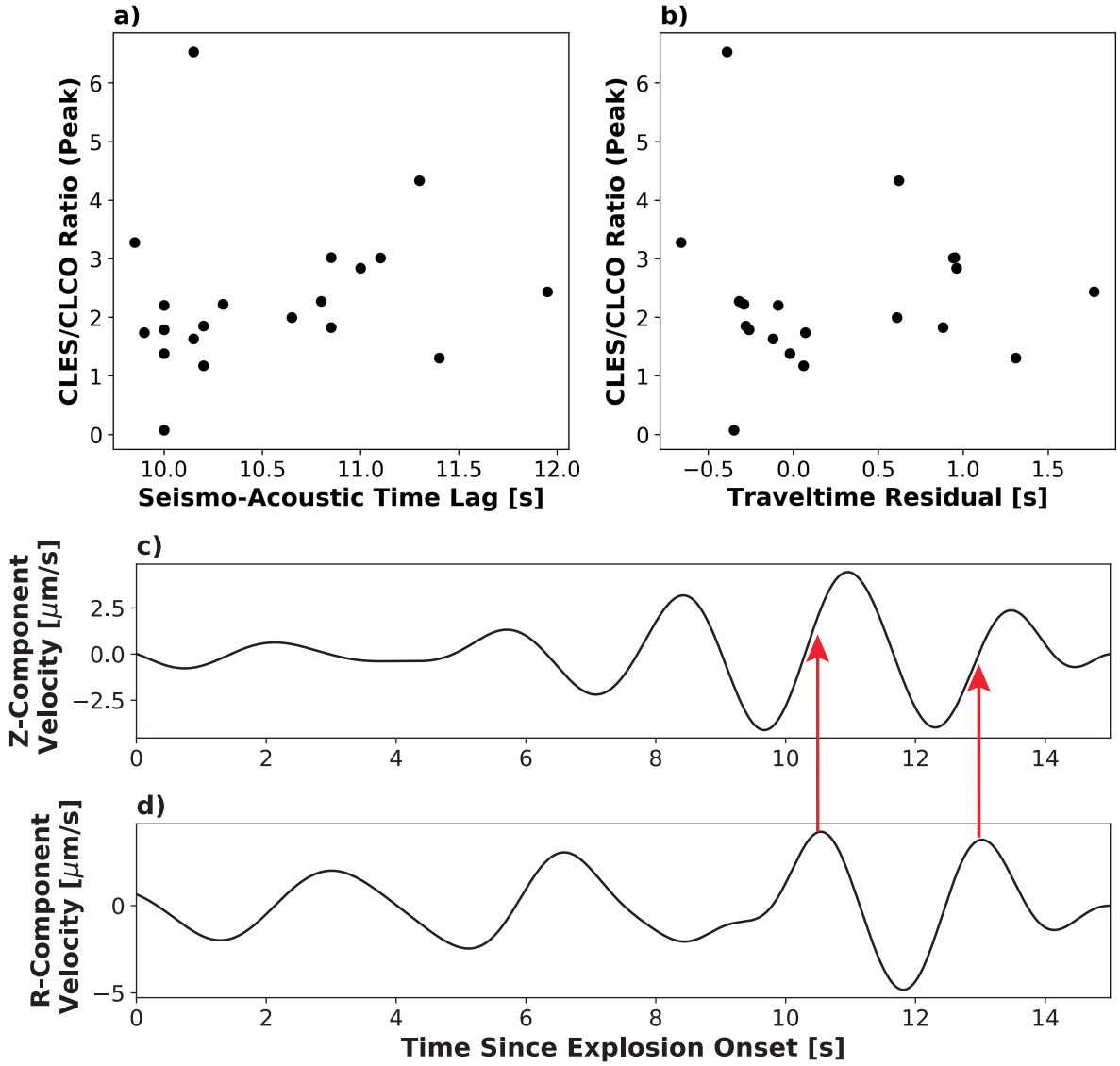

Figure S3. Peak amplitude ratio in the 0.25 - 0.5 Hz range between CLES and CLCO. Amplitude ratio consists of the peak displacement on the east component of the 1.5 s surrounding the p-wave on CLES and the 5 s surrounding the onset of the Rayleigh wave on CLCO. The amplitude ratio is plotted against **(a)** the seismo-acoustic time lag and **(b)** the travel time residual, showing little to no correlation. The **(c)** vertical and **(d)** radial components of the CLCO data show the Rayleigh wave with 90 degree phase shift, as highlighted by the red arrows.

1.1.4 Wind Noise

We account for the lack of in-situ wind conditions using both model-based (AVO-G2S) and data-based (leveraging onset times between CLES and CLCO) methods to calculate the effective sound speed for each explosion (c_{eff}). We chose to use the data-based method for subsequent analyses in the study because it best accounts for changes in atmospheric conditions.

To further investigate the effect of wind, we follow the methods of Fee and Garces (2007) for looking at the low frequency (0.02-0.3 Hz) component of infrasound for each explosion. This type of analysis shows essentially the "magnitude of noise", whereas the c_{eff} calculations that we are interested in also account for directionality of the wind conditions. We show the power spectral density (PSD) for the 60 minutes of CLES infrasound data prior to each explosion using 60 s windows with 50% overlap (Figure S4).

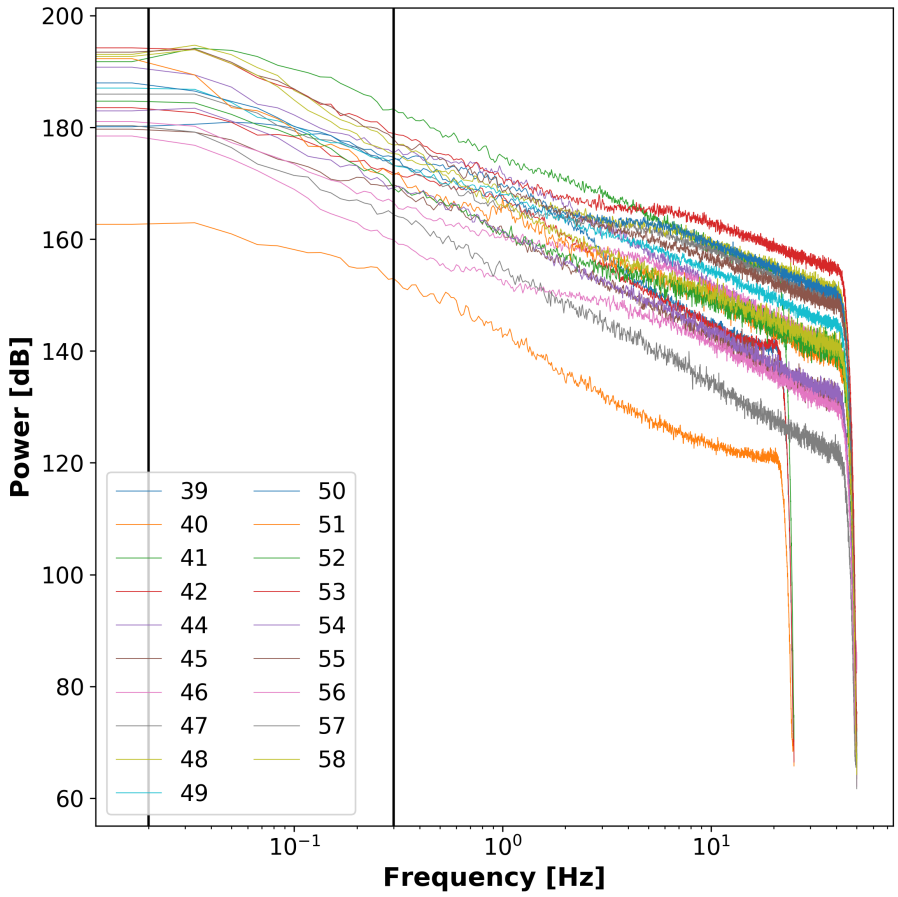

Figure S4. power spectral density (PSD) for the 60 minutes of CLES infrasound data prior to each explosion. The PSD uses 60 s windows with 50% overlap for the calculations, with vertical lines denoting the 0.02-0.3 Hz frequency band used as a proxy for wind noise in Fee and Garces (2007).

REFERENCES

Bath, M. (1985). Surface-wave magnitude corrections for intermediate and deep earthquakes. *Physics of the Earth and Planetary Interiors* 37. doi:10.1016/0031-9201(85)90010-X

Fee, D. and Garces, M. (2007). Infrasonic tremor in the diffraction zone. *Geophysical Research Letters* 34. doi:10.1029/2007GL030616

Haney, M., Lyons, J., Power, J., and Roman, D. (2019). Moment Tensors of Small Vulcanian Explosions at Mount Cleveland, Alaska. *AGU Fall Meeting 2019, V41A-05*